International Journal of Heat and Mass Transfer 224 (2024) 125300

Contents lists available at ScienceDirect

International Journal of Heat and Mass Transfer

journal homepage: www.elsevier.com/locate/ijhmt

Experimental and theoretical investigation of the Leidenfrost dynamics of solid carbon dioxide discs sublimating on a solid substrate

A.S. Purandare [a,*,1], C. Cuartas-Vélez [b,*,1], N. Smeman [a], M. Schremb [a], N. Bosschaart [b], S. Vanapalli [a,*]

[a] Applied Thermal Sciences laboratory, Faculty of Science and Technology, University of Twente, Post Bus 217, 7500 AE Enschede, the Netherlands
[b] Biomedical Photonic Imaging Group, Faculty of Science and Technology, University of Twente, Post Bus 217, 7500 AE Enschede, the Netherlands

ARTICLE INFO

Keywords:
Leidenfrost effect
Dry ice
Sublimation
Optical coherence tomography

ABSTRACT

Volatile liquid droplets levitate on a cushion of their vapor when placed on a hot solid substrate. While extensive research has focused on investigating this phenomenon, commonly known as the Leidenfrost effect in the context of liquids, it may also occur for solids whose triple point pressure is above normal ambient conditions. The present study experimentally and theoretically investigates the Leidenfrost effect for a disc-shaped dry ice pellet placed on a temperature-controlled hot sapphire substrate. The spatial and temporal evolution of the vapor layer thickness below the pellet is measured for varying substrate temperatures using optical coherence tomography (OCT). Simultaneously, the shrinkage of the sublimating dry ice pellet is recorded using video cameras. It is shown that the bottom surface of the pellet is approximately flat within the surface roughness and the resolution of the experimental setup. Intriguingly, this study reveals that the vapor layer thickness below a Leidenfrost solid increases with time in contrast to the dynamics observed for a Leidenfrost liquid droplet/puddle. Additionally, a theoretical model based on the lubrication approximation is employed to estimate the vapor layer thickness and the temporal evolution of the pellet's geometry. The theoretical predictions generally agree well with the measurements throughout the majority of the pellet's lifespan, with deviations observed towards the end of its sublimation due to the assumption of a constant pellet diameter in the model. Furthermore, the theoretical predictions reasonably represent the pellet's lifetime across a wide range of substrate temperatures, validating the predictive capabilities of the theoretical model in the present scenario.

Nomenclature

ΔT	Degree of superheat [K]
δ	Vapor layer thickness [m]
δ^*	Dimensionless vapor layer thickness
δ_0^*	Initial dimensionless vapor layer thickness
$\dot{m}$	Sublimation rate [kg/s]
$\dot{m}''$	Sublimative mass flux [kg/(m^2 s)]
ϵ^*	Sublimation number
$\mathcal{E}$	Evaporation number
μ_v	Dynamic viscosity of CO2 vapor [kg/(m s)]
ν_v	Kinematic viscosity of CO2 vapor [m^2/s]
ρ_s	Density of dry ice pellet [kg/m^3]
ρ_v	Density of CO2 vapor [kg/m^3]
$\rho_{v,sat}$	Vapor density at saturation temperature [kg/m^3]
σ	Stefan-Boltzmann constant [W/(m^2 K^4)]
τ	Time constant [s]
d_i	Dry ice pellet diameter [m]
F	Force exerted by vapor layer [N]
g	Acceleration due to gravity [m/s^2]
h_i	Dry ice pellet height [m]
h_{center}	Pocket region thickness in Leidenfrost drops [m]
$h_{i,0}$	Initial dry ice pellet height [m]
h_{neck}	Neck region thickness in Leidenfrost drops [m]
k_v	Thermal conductivity of CO_2 vapor [W/(m K)]
L	Specific latent heat of dry ice [J/kg]
m	Dry ice pellet mass [m]
p	Vapor pressure [N/m^2]
T_i	Dry ice pellet temperature [K]
T_p	Substrate temperature [K]

* Corresponding authors.
E-mail addresses: a.s.purandare@utwente.nl (A.S. Purandare), c.a.cuartasvelez@utwente.nl (C. Cuartas-Vélez), s.vanapalli@utwente.nl (S. Vanapalli).
[1] These authors contributed equally to this work.

https://doi.org/10.1016/j.ijheatmasstransfer.2024.125300
Received 2 June 2023; Received in revised form 6 January 2024; Accepted 6 February 2024
Available online 20 February 2024

v_r Radial component of vapor velocity [m/s]
v_z Axial component of vapor velocity [m/s]

1. Introduction

A volatile liquid droplet may hover on a cushion of its own vapor above a surface at a temperature significantly exceeding the saturation temperature of the droplet, which is commonly referred to as the Leidenfrost effect [1–4]. In that situation, the evaporative flux of the liquid in close vicinity to the relatively hot substrate prevents the liquid from direct contact with the substrate. Although the origin of the Leidenfrost effect is, in principle, well understood, more specific phenomena involved are still a subject of ongoing research [1]. Recent advances, for example, include the theoretical prediction of the vapor layer geometry [5], the onset of the Leidenfrost effect [6], the self-propelling nature [7], impact dynamics [8], and trampolining of Leidenfrost drops [9].

Materials with a triple point pressure above ambient conditions may exhibit a similar phenomenon when interacting with a surface whose temperature surpasses the saturation temperature of the material at ambient pressure. A common example of this phenomenon is carbon dioxide, having a triple point pressure and temperature of 5.1 atmospheres and −56.5 °C, respectively. Since ambient conditions prevent the existence of liquid carbon dioxide, solid carbon dioxide, also known as dry ice, sublimates at −78.5 °C under a saturated environment at atmospheric pressure. The low temperature and non-existence of a liquid state at ambient conditions facilitate several applications for dry ice, such as cleaning telescope mirrors and semiconductor wafers [10], spray cooling to freeze food and pharmaceutical products [11–13], closed cycle refrigeration [14], cloud seeding [15], and energy harvesting [16].

Although the fundamental origin of the Leidenfrost effect might be the same as in the case of a Leidenfrost droplet, the Leidenfrost dynamics of a Leidenfrost solid are expected to differ from that of liquids due to the absence of capillary and convective effects. In both cases, a key parameter within the Leidenfrost effect is the thickness of the vapor layer as it controls the vapor pressure, heat transfer rate, and flow profile below the Leidenfrost object. For liquid droplets, extensive research has been conducted to investigate the Leidenfrost phenomenon both experimentally and theoretically. The vapor layer thickness for liquid droplets has been modeled within the scope of lubrication theory [5,7,17] and measured using techniques such as X-ray imaging [18], laser diffraction [19], and interferometric methods [20]. Specific features associated with the Leidenfrost effect, such as controlled droplet mobility on ratchets [21,22] and trampolining [9] have also been studied in the context of liquid droplets. However, the investigation of the Leidenfrost phenomenon for solids like dry ice has been limited to studying their propulsion on structured surfaces [23–25]. Currently, there is a lack of direct measurement and theoretical modeling of the vapor layer thickness beneath Leidenfrost solids in the existing literature. The presence of the vapor layer significantly reduces the cooling efficiency, which has large implications for ensuring reliable temperature control and cleaning processes in various industrial applications. Therefore, the vapor layer thickness is a crucial parameter when considering the interaction between a Leidenfrost solid object and the underlying substrate.

In the present work, the Leidenfrost effect for a disc-shaped dry ice pellet placed on a hot solid substrate is investigated, both theoretically and experimentally. Experimental measurements are conducted by placing dry ice pellets on a temperature-controlled sapphire substrate. The thickness of the vapor layer beneath the pellet is determined using optical coherence tomography (OCT) at five different substrate temperatures. This enables precise spatial and temporal measurements of the vapor layer thickness. Additionally, video cameras are used to record the evolution of the pellet's shape. Further experiments are conducted outside the OCT setup to explore a wider range of substrate temperatures and measure the lifespan of the dry ice pellet on an aluminium substrate. To model the dynamics of the vapor layer thickness and the sublimation of the dry ice pellet, the lubrication approximation is employed, assuming a uniform vapor layer thickness and a constant pellet diameter. An overall comparison of the predicted and measured values of the pellet's lifetime, the temporal evolution of the vapor layer thickness, and the pellet's geometry reveal good agreement for the majority of the pellet's lifespan. The findings of the present study provide quantitative insight into the Leidenfrost dynamics of dry ice pellets, which have potential implications for various industrial applications.

2. Experimental

The investigation conducted in this paper is substantiated by a comprehensive comparison with experimental data. The subsequent subsections provide detailed explanations of the experimental setups employed for measurements and the methodology used in this study.

2.1. Dry ice pellets

In the first step, a large dry ice block with a diameter of 7 cm and a height of 3 cm is produced using a commercially available dry ice pellet generator (CARBONEIGE 100, Air Liquide [26], France) in which a low-density, inhomogeneous and porous pellet is formed. The dry ice block is crumbled and the resulting dry ice fragments are die-forged into smaller disc-shaped pellets with a diameter of 10 mm and a height of 5 mm. The effective average density of the pellets ranges $1005 - 1020\ \mathrm{kgm^{-3}}$, as calculated from the volume and mass at the beginning of every experiment. It is important to note that moisture present in the ambient may condense and freeze in the dry ice and eventually be trapped inside the pellet while it is being produced. Care is taken in order to limit that influence by minimizing the time during which the dry ice pellet is exposed to ambient air. However, water ice crystals being entrapped inside the dry ice pellet cannot be completely ruled out. By using tweezers with insulated tips, the disc-shaped dry ice pellets are gently placed on a disc-shaped sapphire substrate (SP: HEM Ti:Sapphire, GT Advanced Technologies, USA) with a diameter and thickness of 90 mm and 11 mm, respectively.

The substrate is heated via three film heaters (H) symmetrically glued on its periphery. The substrate temperature is measured with two PT1000 sensors (T_n and T_p) attached to the top of the substrate, as close as possible to the position of the pellet. The power supply of the heaters is controlled with a PID controller (Model 336, Lake Shore Cryotronics, USA). To ensure that the substrate temperature is homogeneous prior to an experiment, a pellet is placed on the substrate after a stabilization period of at least 8 min. Once the system has reached the desired temperature, a retaining ring, displayed in the inset of Fig. 1, is placed on the substrate to gently restrict the movement of the pellet during the experiment. While restricting the movement of the pellet, the retaining ring also induces a reaction force to oppose the movement of the pellet. This, in turn, may induce an inclination between the pellet and the sapphire substrate as speculated and discussed in Section 4.2.

2.2. OCT system

Once the dry ice pellet has been placed, the vapor layer thickness is measured using a custom-built optical coherence tomography (OCT) system depicted in Fig. 1 and described in previous work [27–29]. The main differences between the system depicted in Fig. 1 and our previous work are the introduction of a galvanometer scanner (GS) for lateral beam scanning and the adaptation to a common-path interferometer [30], rather than a classic Michelson interferometer. This simple adaptation was achieved by introducing a beam blocker (BB) in the reference path of the interferometer.

In the system, light from a supercontinuum broadband source (SuperK EXTREME EXB-6, NKT Photonics, Denmark) propagates through two density filters and three lenses (L1: LD2746-A, L2: LD2060-A, L3:

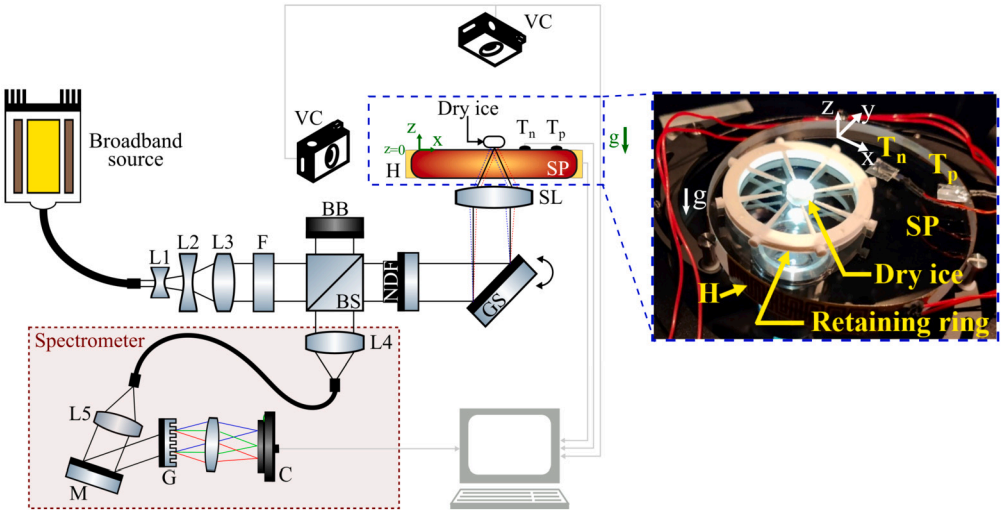

Fig. 1. Schematic of the experimental setup employing OCT to measure the vapor layer thickness between a disc-shaped dry ice pellet and a heated sapphire substrate. The snippet in the figure shows the test section of the OCT setup where the dry ice pellet is placed on a heated sapphire substrate and held using a retaining ring. L1-L5: lenses, BS: beam splitter, BB: beam blocker, NDF: neutral density filter, GS: galvanometer scanner, SL: scanning lens, SP: sapphire substrate, H: heater, T_n-T_p: temperature sensors, M: mirror, G: grating, C: line camera, VC: video camera, g: gravity.

LB1471-A, Thorlabs, USA) that attenuate, expand and collimate the beam. Wavelengths above 700 nm are filtered by a short-pass filter (F: FESH0700, Thorlabs, USA) before the light arrives at a 10:90 beam splitter (BS: BS028, Thorlabs, USA). From the incoming beam, 90% of the light is guided towards a beam blocker which completely attenuates the beam, and the remaining 10% is transmitted towards the dry ice.

Light propagating to the dry ice from the BS is attenuated by a neutral density filter (NDF: NDC-50C-2M-A, Thorlabs, USA) that limits the total delivered power to ≈ 5 mW. A galvanometer scanner (GS: 8320K, Cambridge Technology, USA) is used to displace the beam in the xy plane, parallel to the bottom of the dry ice and perpendicular to the direction of beam propagation z (as shown in Fig. 1), over an area of 4 mm × 4 mm with a sampling of 256 points along each axis, leading to an in-plane spacing of ≈ 15.6 μm. After the galvanometer scanner, light is focused after the sapphire substrate by a scanning lens (SL: LSM03-VIS, Thorlabs, USA) with a focal length of 39 mm.

The sapphire substrate is located between the scanning lens and the dry ice. The reflection at the interface between the sapphire disc and the vapor layer acts as the reference path (≈ 7.7% of the incoming light). This configuration is equivalent to that of a common-path interferometer [30], where the reference optical path and the sample optical path are coaligned. The main advantage of this common-path configuration is greater stability due to the coincidence of the sample and reference paths [30]. The interference between light back-scattered by the dry ice pellet (sample) and the reflection at the interface of the sapphire substrate and the vapor layer (reference) is used to reconstruct the OCT scans. The light that is collected back into the optical system is reflected at the BS to a custom-built spectrometer (HoloSpec f/1.8i, Kaiser Optical Systems, USA) through a single-mode fiber (S405XP, Thorlabs, USA). In the spectrometer, light is dispersed by a grating (G) on a line camera (C: Sprint spL4096-140km, Basler, Germany) which has an acquisition rate of 16.6 kHz and an exposure time of 58 μs. The spectrum collected ranges 480 – 660 nm with a resolution of 0.1 nm and has a full width at half-maximum of ≈ 90 nm centered at ≈ 570 nm, implying a theoretical axial (z-axis) resolution of ≈ 1.6 μm in air (≈ 1.7 μm measured experimentally) and a z-axis range of ≈ 0.9 mm. The lateral (xy-axis) resolution of the system given by the scanning lens is ≈ 7 μm.

In addition to the OCT system, two video cameras (VC), located at the top and in front of the pellet, are used to track the changes in the geometry of the dry ice pellet. Both cameras have a set exposure of ≈ 0.5 ms and are triggered every ≈ 1.1 s during acquisition in synchrony with the OCT system.

2.2.1. Data acquisition

During the lifespan of the dry ice, OCT scans and camera videos are recorded simultaneously. For the OCT acquisition, a data acquisition system (USB-6211, National Instruments, USA) is used to control the galvanometer scanner and to trigger the camera at the spectrometer. Acquisition of a cross-sectional scan in the xz-plane (4 mm×0.9 mm) takes ≈ 0.17 s while an entire OCT volume scan with 4 mm×4 mm×0.9 mm (xyz) takes ≈ 45 s. During the acquisition, two imaging schemes are used. In the first scheme, 4 volume scans are acquired during the lifespan of the dry ice, in the second scheme, cross-sectional scans, without displacement along the y-axis, are recorded at the middle of the acquisition scan (as indicated with a dashed line in Fig. 4(c)). A detailed explanation of the acquisition modalities can be found in Supplementary Material - Section 1. The two video cameras are triggered simultaneously one time after eight xz-planes are acquired. Since the area scanned by the OCT system is smaller than the pellet's bottom area, the measurement of the vapor layer thickness is susceptible to errors due to the pellet's movement. Therefore, the retaining ring restricts the movement of the pellet to a similar location for each experiment during the pellet's lifetime.

2.2.2. Data processing

A detailed overview of the analysis procedure for the data from the OCT system is described in our previous work [28,29] and in Supplementary Material - Section 1. Briefly, the interference pattern obtained at the spectrometer is processed by subtracting the background, interpolating wavelength into wavenumber, and applying Fourier transform. The resulting signal is an intensity pattern as a function of the z-axis (as depicted in Fig. 4(a)). This procedure is continuously repeated for each scan when traversing in the xy plane during the lifetime of the dry ice. The resulting dataset is the intensity as a function of the xyz-axes and time. The 2D images are created by displaying two orthogonal directions (as in Fig. 4(b)), and the 3D view is created as a projection of the three axes (as in Fig. 4(c)). From the intensity profiles, the distance between the peak intensity and the origin of the z-axis determines the vapor layer thickness.

The measurement of the temporal evolution of the vapor layer is based on unidirectional scans in the x-direction. A line with a length of 2 mm positioned at the center of the dry ice is taken and analyzed by measuring the average vapor layer thickness and the standard deviation (SD) (Fig. 5(a)). The averaged vapor layer thickness and SD within this region are calculated during the dry ice lifetime (as presented in

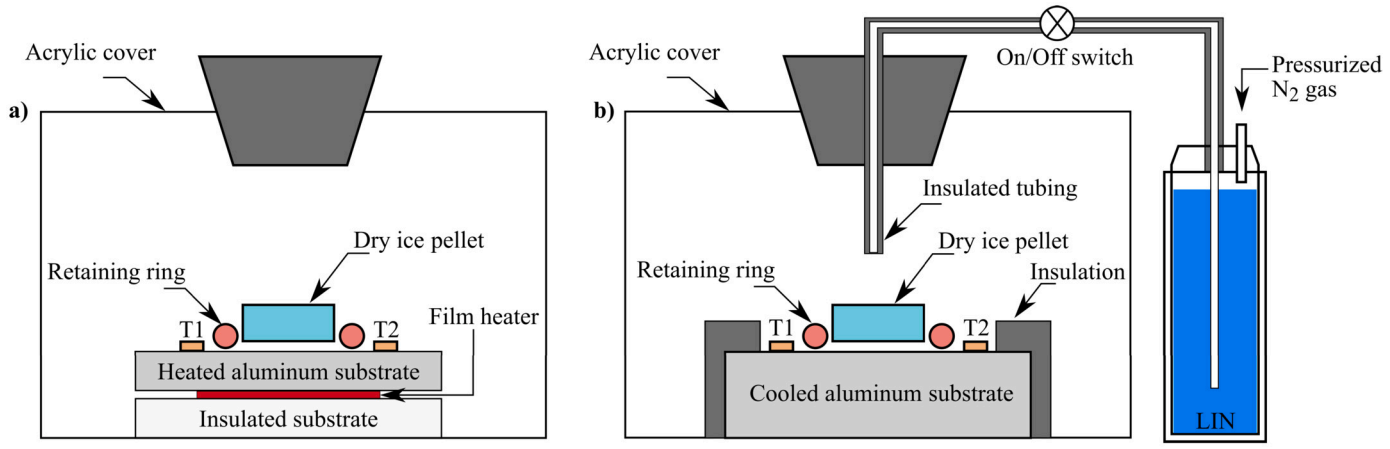

Fig. 2. a) Schematic of the experimental setup used to visually measure the lifetime of a disc-shaped dry ice pellet placed on an aluminum substrate heated above ambient temperature using a thin film heater. **b)** Schematic of the experimental setup used to visually measure the lifetime of a disc-shaped dry ice pellet placed on an aluminum substrate cooled down below ambient temperature using a spray of liquid nitrogen prior to the experiment. In both cases, the pellet is gently placed on the substrate and it is held in position using a retaining ring. The temperature of the substrate is measured with two thermocouples, T_1 and T_2, attached to the top of the substrate.

Fig. 5(b)). The pellet height and diameter over time are obtained from the data from the front-view video camera by tracking grayscale intensities of the front-view images in the vertical and horizontal directions. Towards the end of its sublimation, the pellet shrinks rapidly, and the corresponding grayscale intensity values are noisy given the limited frame rate and resolution of the video cameras. The outliers in the measured values of the grayscale intensities of the front view images are neglected and the data is presented as a curve fitted through the grays scale values with 95% confidence intervals (CI) for the fitted parameters.

2.3. Dry ice pellet lifetime measurement

The temperature of the sapphire substrate used in the OCT setup varied from ≈ 303 K to ≈ 343 K. In order to facilitate a wider substrate temperature range and study its influence on the lifetime of the dry ice pellet, measurements are performed outside the OCT setup. For this purpose, an aluminum substrate is used and its temperature is varied from ≈ 205 K to ≈ 418 K. The schematic of the setup is shown in Fig. 2. For temperatures higher than ambient, the aluminum substrate is heated with a thin film heater glued on the bottom face of the substrate, as shown in Fig. 2(a). A PID controller implemented in LabVIEW is used to regulate the electrical input of the heater based on the substrate temperature as measured with two thermocouples (T_1 and T_2) attached on either side of the pellet, as close as possible to it. The pellet is surrounded by a retaining ring which gently restricts the pellet's movement during the experiment.

For temperatures lower than ambient, the substrate is first cooled by liquid nitrogen which is sprayed on the substrate by applying pressure to a vacuum-insulated flask containing liquid nitrogen (see Fig. 2 (b)). The temperature is monitored during the cool down of the substrate. The spray of liquid nitrogen is switched off when the desired substrate temperature is reached and the pellet is gently placed on the substrate. The aluminum substrate is insulated on its periphery to reduce heat leaks. In the case of low-temperature measurements, the temperature of the substrate was not actively controlled, causing the temperature to increase at the rate of ≈ 0.3 $\mathrm{K\,min^{-1}}$ due to the heat capacity of the substrate. For instance, the lifetime of the pellet for an initial substrate temperature of ≈ 205 K was ≈ 14 min during which the substrate temperature would have increased by ≈ 4.5 K. For such cases, the substrate temperature is averaged over the time period of an experiment, and the pellet's lifetime is shown as a function of the mean substrate temperature and ± SD.

The pellets used in these measurements were produced in a similar way described in Section 2.1. The initial diameter, height, and mean density of the pellets were 10 mm, 5 mm, and ≈ 1019 $\mathrm{kgm^{-3}}$, respectively. The mass of the pellet at the start of every experiment fell in the range 313 ± 3.7 mg (95% confidence interval). A manual digital stopwatch was used to record the time to complete visual sublimation of the pellet. In order to check the repeatability of the experiment, three dry ice pellets were measured for every substrate temperature.

3. Formulation of the model

The theoretical model used to describe the Leidenfrost state of a dry ice disc on a hot substrate is based on the geometrical situation schematically shown in Fig. 3, and six basic assumptions in relation to the dry ice pellet and the hot substrate, which are: *i*) The problem is axisymmetric since the dry ice pellet under consideration is disc-shaped. *ii*) The dry ice pellet sublimates at a constant temperature of 195 K under standard ambient conditions. *iii*) Sublimation occurs quasi-steady where the sublimation enthalpy of dry ice is ≈ 571 kJ/kg. *iv*) The vapor layer thickness is uniform below the pellet. *v*) The substrate is isothermal. *vi*) The radiative heat flux through the vapor layer is negligible compared to the conductive heat flux, as the latter is two orders of magnitude higher than the former $\left(\sigma(T_p^4 - T_i^4)/\bar{k_v}\frac{T_p - T_i}{\delta} \approx 0.01\right)$, where $\sigma = 5.67 \times 10^{-8}$ $\mathrm{W/(m^2\,K^4)}$ is the Stefan-Boltzmann constant, $\bar{k_v} \approx 12.5$ mW/(m K) is the thermal conductivity of CO_2 vapor, and $T_p \approx 303$ K and $T_i \approx 195$ K are the substrate and dry ice temperature, respectively. Based on these assumptions, first we model the situation for the steady-state case of a constant dry ice geometry, followed by the prediction of the temporal evolution of the system assuming quasi-steady sublimation.

3.1. Steady-state geometrical model

In order to describe the steady-state case for a dry ice pellet in the Leidenfrost state on a hot substrate, the coupled momentum, heat, and mass transfer problem is solved to predict the vapor layer thickness below the pellet. The flow in the vapor layer below the pellet is described in the framework of the lubrication theory since the vapor layer thickness is much smaller than the diameter of the pellet, $\delta \ll d_i$ [24]. In this context, the momentum balance in the vapor layer is given by

$$\frac{1}{\rho_v}\frac{\partial p}{\partial r} = \nu_v \frac{\partial^2 v_r}{\partial z^2}, \tag{1}$$

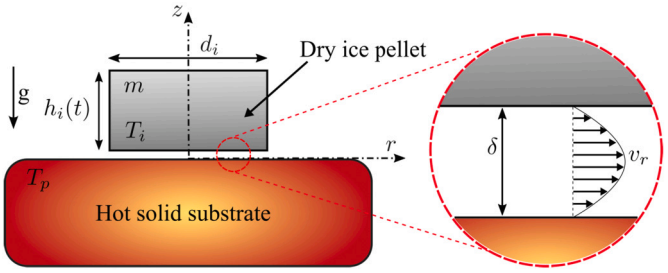

Fig. 3. Schematic of the geometric situation considered for the theoretical description of the Leidenfrost effect for a dry ice pellet on a hot substrate. A disc-shaped dry ice pellet (diameter d_i, height h_i and mass m) at the sublimation temperature T_i hovers on a layer of its own vapor with thickness δ above a hot isothermal solid substrate at temperature T_p. The snippet in the figure schematically shows the vapor layer and the assumed vapor velocity profile.

where p is the pressure, r and z denote the radial and axial coordinates, v_r is the radial component of the vapor velocity, and ρ_v and ν_v are the density and kinematic viscosity of the vapor, respectively.

The CO_2 vapor generated during sublimation at the bottom of the pellet (at depth $z = \delta$) feeds the flow below the pellet and leaves the vapor layer through its periphery. Assuming a constant sublimative mass flux along the pellet's bottom, $\dot{m}''$, mass conservation of the vapor in the flow below the pellet results in

$$\dot{m}''\pi r^2 = \rho_v 2\pi r\delta\bar{v}_r, \tag{2}$$

where $\bar{v}_r = \frac{1}{\delta}\int_0^\delta v_r \mathrm{d}z$ is the average vapor velocity in the vapor layer at a given radial position. From Eq. (2), the radial vapor velocity v_r is proportional to the radial position r, and from Eq. (1), v_r is proportional to axial position $z + z^2$. Therefore, to satisfy both Eq. (1) and Eq. (2) the radial velocity profile must be in the form

$$v_r = \left(Az + Bz^2\right) r. \tag{3}$$

Equation (3) is similar to the one obtained by Castanet et al. [17] while deriving the expression for radial velocity profile velocity below a Leidenfrost liquid puddle.

The constants A and B in the Eq. (3) are obtained using Eq. (2), the continuity equation and the velocity boundary conditions

$$v_r|_{z=\delta} = 0, \quad \text{and} \quad v_z|_{z=\delta} = -\frac{\dot{m}''}{\rho_{v,sat}}, \tag{4}$$

as

$$A = \frac{3\dot{m}''}{\delta^2\rho_{v,sat}}, \quad \text{and} \quad B = \frac{-3\dot{m}''}{\delta^3\rho_{v,sat}}, \tag{5}$$

where, $\rho_{v,sat}$ is the density of the vapor at the saturation temperature of the dry ice pellet. The vapor velocity in the axial direction v_z is obtained from the continuity equation as $v_z = -\int \frac{1}{r}\left(\frac{\partial r v_r}{\partial r}\right)\mathrm{d}z$.

Considering the conduction in the vertical direction as the only heat transfer mechanism between the pellet and the substrate across the vapor layer, the sublimative mass flux, $\dot{m}''$, is related to the vapor layer thickness as

$$-\frac{\bar{k_v}\Delta T}{\delta} = \dot{m}'' L, \tag{6}$$

where $\bar{k_v}$ is the average thermal conductivity of the vapor evaluated at the mean of the temperatures of the substrate and the pellet. In the current situation, the use of the average thermal conductivity to describe the heat flux is justified because the thermal conductivity of the CO_2 vapor between T_p and T_i varies approximately linearly with temperature.

Integrating Eq. (1) and assuming ambient pressure in the flow at the edge of the dry ice pellet, $p = 0$ at $r = d_i/2$, yields the pressure profile inside the vapor layer as

$$p(r) = \bar{\mu_v} B\left(r^2 - \frac{d_i^2}{4}\right), \tag{7}$$

where $\bar{\mu_v}$ is the dynamic viscosity of the vapor evaluated at the mean of the substrate and dry ice temperature. Balancing the force exerted by the vapor layer on the dry ice bottom, which is obtained from integrating the pressure profile as

$$F = -\frac{\pi}{32}\bar{\mu_v} B d_i^4, \tag{8}$$

with the weight of the pellet, $\frac{\pi}{4}\rho_s d_i^2 g h_i$, (where g is the gravitational constant and ρ_s is the dry ice density), the steady-state vapor layer thickness δ is given by

$$\delta = \left(\frac{3}{2}\frac{\bar{\mu_v}\bar{k_v}\Delta T}{L\rho_s g h_i \rho_{v,sat}}\right)^{\frac{1}{4}}\left(\frac{d_i}{2}\right)^{\frac{1}{2}}. \tag{9}$$

This expression for the vapor layer thickness is almost the same as the equation for the thickness of vapor layers below Leidenfrost liquid droplets as previously derived by Biance et al. [19] and Castanet et al. [17], with a difference in the numeric factor in the expression. This difference results from the height of the droplet, which is assumed as two times the capillary length of the droplet liquid in previous works, whereas for the current case the approximate value of the initial pellet height is known.

The vapor layer thickness can be non-dimensional using the pellet diameter. The resulting expression for the dimensionless vapor layer thickness (δ^*) is given by

$$\delta^* = \epsilon^{*\frac{1}{4}}, \tag{10}$$

where

$$\epsilon^* = \frac{3}{8}\frac{\bar{\mu_v}\bar{k_v}\Delta T}{L\rho_s g h_i \rho_{v,sat} d_i^2}. \tag{11}$$

The dimensionless vapor layer thickness is remarkably a function of the dimensionless parameter, ϵ^*. This parameter is termed the sublimation number which refers to a similar parameter (evaporation number $\mathcal{E}$) appearing in the theoretical analysis of Leidenfrost drops in the work by Sobac et al. [5,7].

Finally, the sublimation rate $\dot{m}$ can be determined using Eq. (6) and (9), yielding

$$\dot{m} = -\pi\left(\frac{3}{2}\frac{\bar{\mu_v}}{\rho_s g h_i \rho_{v,sat}}\right)^{-\frac{1}{4}}\left(\frac{\bar{k_v}\Delta T}{L}\right)^{\frac{3}{4}}\left(\frac{d_i}{2}\right)^{\frac{3}{2}}. \tag{12}$$

3.2. Sublimating dry ice pellet

To study the transient evolution of the vapor layer thickness and sublimation rate, the time variation of the pellet geometry is investigated. In this case, the relationship between the pellet height and the vapor layer thickness is assumed to be described as in Eq. (9), and only the pellet's height decreases over time while its diameter remains constant. The last assumption is valid for the majority of the dry ice lifetime (especially for lower substrate temperatures), except towards the end of the sublimation process when the dry ice pellet significantly shrinks in the radial direction as observed during the experiments (see Fig. 5(b)). With that consideration, the transient evolution of the pellet height and the vapor layer thickness during the majority of the sublimation process are analyzed. The sublimation rate of the dry ice pellet is written in terms of the rate of change of its height as

$$\frac{\mathrm{d}m}{\mathrm{d}t} = \frac{\mathrm{d}m}{\mathrm{d}h_i}\frac{\mathrm{d}h_i}{\mathrm{d}t}. \tag{13}$$

Using Eq. (12), (13), and $\frac{\mathrm{d}m}{\mathrm{d}h_i} = \pi\frac{d_i^2}{4}$, the rate of change of the pellet height can be expressed as

$$\frac{\mathrm{d}h_i}{\mathrm{d}t} = -\left(\frac{8}{3}\frac{g\rho_{v,sat}}{\bar{\mu}_v}\right)^{\frac{1}{4}}\left(\frac{\bar{k}_v\Delta T}{d_i^{\frac{2}{3}}\rho_s L}\right)^{\frac{3}{4}} h_i^{\frac{1}{4}}. \tag{14}$$

By integrating Eq. (14), the time dependence of the pellet height $h_i(t)$ is obtained as

$$h_i(t) = h_{i,0}\left(1 - \frac{t}{\tau}\right)^{\frac{4}{3}}, \tag{15}$$

where $h_{i,0}$ is the initial height of the pellet and τ is a characteristic time constant defined as

$$\tau = \frac{4}{3}\left(\frac{3}{8}\frac{\bar{\mu}_v}{g\rho_{v,sat}}\right)^{\frac{1}{4}}\left(\frac{d_i^{\frac{2}{3}}\rho_s h_{i,0} L}{\bar{k}_v\Delta T}\right)^{\frac{3}{4}}, \tag{16}$$

which incorporates the effect of the geometric, thermodynamic, and fluid dynamic parameters controlling the process.

By substituting Eq. (15) in Eq. (9) and using Eq. (11), the time evolution of the vapor layer thickness $\delta(t)$ and its dimensionless form $\delta^*(t)$ are respectively described by

$$\delta(t) = \left(\frac{3}{2}\frac{\bar{\mu}_v\bar{k}_v\Delta T}{L\rho_s g h_{i,0}\rho_{v,sat}}\right)^{\frac{1}{4}}\left(\frac{d_i}{2}\right)^{\frac{1}{2}}\left(1 - \frac{t}{\tau}\right)^{-\frac{1}{3}} \tag{17}$$

and

$$\delta^*(t) = \epsilon^{*\frac{1}{4}}\left(1 - \frac{t}{\tau}\right)^{-\frac{1}{3}}. \tag{18}$$

Note that Eq. (18) reduces to Eq. (10) at the initial time, i.e. when $t \to 0$. The scaling for the temporal evolution of the vapor layer thickness below a disc-shaped dry ice pellet is found as $\delta \sim \left(1 - \frac{t}{\tau}\right)^{-\frac{1}{3}}$. In contrast, Biance et al. [19] predicted and measured a linearly decreasing relationship $\delta \sim \left(1 - \frac{t}{\tau'}\right)$ for sessile Leidenfrost drops.

4. Results

4.1. OCT measurement data

A dry ice pellet with an initial diameter $d_i = 10$ mm and height $h_i = 5$ mm is gently placed on a smooth sapphire substrate whose temperature is controlled to a fixed value significantly above the sublimation temperature of dry ice. Consequently, the pellet, with an initial mass of $m \approx 375$ mg, hovers on a cushioning layer of its own vapor until it is completely sublimated after approximately $\tau \approx 130$ s on a substrate at a temperature $T_p \approx 313$ K. During the pellet's lifetime, the geometry of the vapor layer below the pellet is continuously characterized using an OCT measurement system.

Example measurements in the form of intensity data obtained using the OCT system are shown in Fig. 4. The intensity profiles along the z-direction acquired at a constant xy location (indicated by a cross mark in Fig. 4(b) and (c)) are presented in Fig. 4(a) for three different times. For each profile, the top surface of the sapphire substrate is located at $z = 0$ μm. The intensity value along the z-axis is maximal at the z-value that corresponds to the bottom surface of the dry ice pellet. Since the vapor layer is enclosed by the sapphire substrate and the bottom surface of the pellet, this z-value at maximum intensity represents the thickness of the vapor layer between the sapphire substrate and the dry ice pellet (δ). As shown in Fig. 4(a), the peak intensity is located at larger depths for increasing time, indicating that the vapor layer thickness increases over time as the dry ice sublimates.

Apart from the major reflections attributed to the macroscopic bottom of the pellet, significant intensity values are also found around the peak intensity. The significant values observed at larger z-positions are ascribed to the light beam partially penetrating into the porous dry ice pellet where light is then reflected back. The intensity signal in the region before the peak intensity, hereafter termed foot region, for a given measurement broadens as the vapor layer thickness increases over time. This behavior may be hypothetically explained by the effect of water-ice particles trapped inside the dry ice pellet during the manufacturing process as described in Section 2.1. In the course of the sublimation of the dry ice pellet, those ice particles are released at the dry ice bottom (as discussed in Section 2 of the Supplementary Material and depicted in the Supplementary **Video File**) and are carried away radially by the vapor flow inside the vapor layer. While the ice particles may distort the measurement through reflections of light inside the vapor layer, the temporal evolution of the flow inside the layer causes growth of the foot region over time. As the vapor layer thickness increases, the heat flux from the substrate to the pellet decreases, resulting in a reduced vapor mass flow rate and velocity. As a consequence, the ice particles experience less radial acceleration leading to a longer residence time and a larger effective penetration into the vapor layer over which they scatter light. Consequently, the increasing width of the foot region in the intensity profiles would represent this increasing penetration of the ice particles.

The 2D cross-sectional views of the pellet in the form of intensity images in different planes generated from a complete OCT volume scan (4 mm×4 mm×0.9 mm in xyz, respectively) are shown in Fig. 4(b). The pronounced bright white lines in the intensity images for the xz and yz planes represent the edge of the dry ice pellet in those respective planes. The gap below the bright line in the xz plane and on the left of the bright line in the yz plane represents the vapor layer thickness between the pellet and the sapphire substrate. The 3D image of a pellet as viewed from the sapphire substrate and reconstructed using the 2D images shown in Fig. 4(b) is displayed in Fig. 4(c). During the volume scan, a part of the curved periphery of the pellet's bottom face is captured as seen in the xy plane of Fig. 4(b). This periphery is visible due to movements of the pellet when initially placed on the substrate. Additionally, as the field of view of the OCT system is smaller than the pellet bottom surface, only a portion of the surface total area is measurable. While the data obtained from volume scans of the dry ice bottom is only used for illustration purposes, the temporal evolution of the vapor layer thickness is quantitatively analyzed based on uni-directional measurements along a line on the bottom face of the pellet in the following section.

4.2. Temporal evolution of the vapor layer thickness

The variation of the vapor layer thickness with time is studied using measurement data for an xz-plane at the center of the y-axis of the OCT acquisition, this is illustrated with a dashed line in Fig. 4(c). Acquisition of a single xz-scan allows a higher sampling rate compared to a complete volume scan, resulting in a sufficient temporal resolution of the measurements when compared to the sublimation time of the dry ice pellet. The measurement data in the xz-plane consists of 256 intensity profiles along the z-axis for the varying positions along the x-axis and its acquisition time (≈ 0.17 s) is three orders of magnitude lower than the typical lifespan of a dry ice pellet ($\sim$ 100 s), allowing a high temporal resolution of the measurement. Fig. 5(a) shows the variation of the vapor layer thickness and the dry ice bottom profile across the x-direction (see dashed line in Fig. 4(c)) at different times, when a pellet of mass $m \approx 403$ mg is sublimating on a sapphire substrate of temperature $T_p \approx 313$ K. In Fig. 5(a), solid lines represent the measured vapor layer thickness, dashed lines correspond to the average vapor layer thickness, and the bands surrounding the average values represent ± standard deviation (SD) of the vapor layer thickness along the x-axis at the respective time. The fluctuations in the vapor layer thickness given by the SD ranged between $2 - 3$ μm which may be attributed to the roughness of the bottom surface of the pellet and the z-axis resolution (≈ 1.7 μm) of the OCT system. Since the deviation of the vapor layer thickness is in the order of the resolution of the system and small

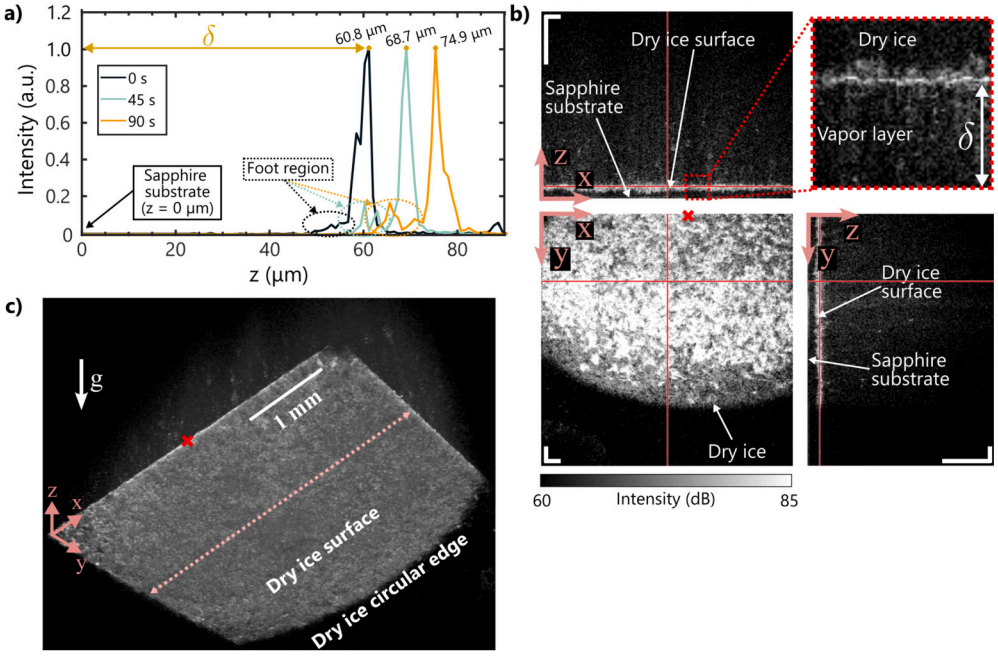

Fig. 4. OCT measurement data for a disc-shaped dry ice pellet (with an initial mass of $m \approx 375$ mg) hovering on a sapphire substrate heated to ≈ 313 K. **a)** Intensity profiles along the z-axis acquired at a constant xy location for three different times. The xy location is indicated with a red cross marker in (b) and (c). The z-position of the intensity peak (golden point markers in **a)**) represents the vapor layer thickness δ. **b)** 2D cross-sectional views obtained after a complete OCT volume scan showing the dry ice bottom surface, the sapphire substrate, and the vapor layer in the xy, xz, and yz planes. Scale bars in the images correspond to 200 μm and the images are presented in logarithmic scale. **c)** Reconstructed 3D view of a volume of 4 mm×4 mm×0.9 mm (xyz) displaying a section of the dry ice pellet using the images shown in (b); g indicates the direction of gravity. (For interpretation of the colors in the figure(s), the reader is referred to the web version of this article.)

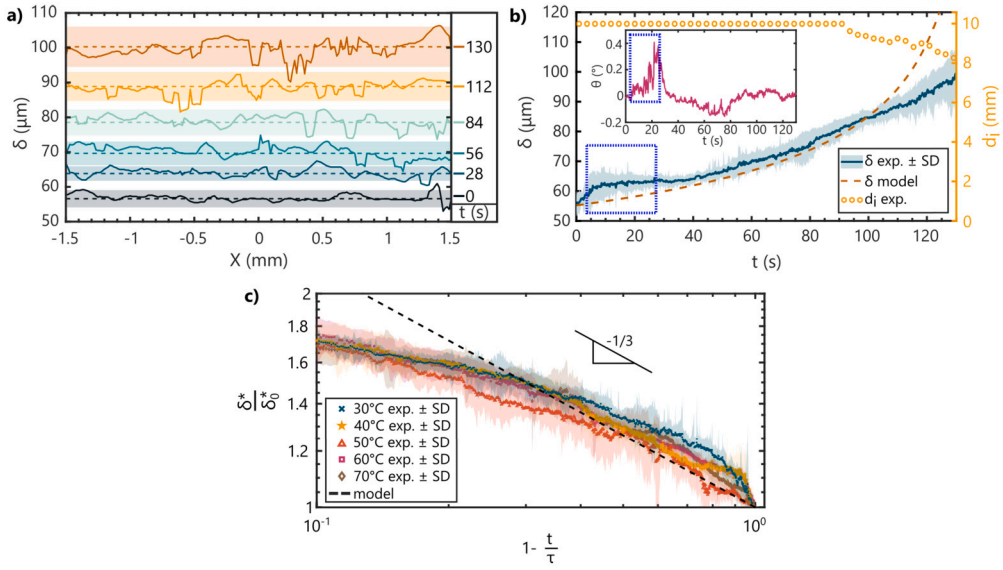

Fig. 5. Vapor layer thickness measurements showing **a)** Measured vapor layer profile along x-direction (dashed line in Fig. 4(a)) below a disc-shaped dry ice pellet (with an initial mass of ≈ 403 mg) placed on a sapphire substrate ($T_p \approx 313$ K) at different times. Solid lines represent the vapor layer thickness, dashed lines represent the vapor layer thickness averaged along the x-axis, and the bands correspond to ± SD. **b)** Predicted and experimental temporal evolution of the vapor layer thickness averaged along the x-axis. The circular symbols represent the measured pellet diameter (d_i). The inset in **b)** shows the time variation of the angle of inclination of the pellet with respect to the sapphire surface. The data shown in **a)** and **b)** for a sapphire substrate temperature of $T_p \approx 303$ K, 323 K, 333 K, and 343 K can be found in Supplementary Material - Section 2. **c)** Dimensionless vapor layer thickness as a function of dimensionless time for various sapphire substrate temperatures in double logarithmic representation.

compared to the mean value, the vapor layer thickness is assumed uniform in the theoretical analysis (Section 3).

The comparison of the measured temporal evolution of the vapor layer thickness with predicted values calculated using Eq. (17) is shown in Fig. 5(b) for the same pellet as in Fig. 5(a). In Fig. 5(b), the solid lines represent the measured average vapor layer thickness along the x-axis, the shaded band corresponds to the $\pm$ SD along an x-axis line (elaborated in Supplementary Material - Section 1), the dashed line indicates the predicted values of the vapor layer thickness, and circular symbols illustrate the measured values of the pellet's diameter. In the measured data of the average vapor layer thickness, an anomalous elevation can be observed during the initial $\approx$ 35 s as highlighted by the dashed box in Fig. 5(b). This observation may be ascribed to the influence of the initial misalignment between the bottom surface of the pellet and the sapphire substrate at the commencement of the experimental procedure. When initially placed, the pellet should ideally be completely parallel to the substrate. However, due to imperfection in the geometry during manufacturing and the reactive force from the retaining ring restricting the pellet's movement, the pellet may become inclined with respect to the sapphire surface. That inclination forms an angle (θ) which changes over time as the dry ice tends to balance the force on the entire surface. The angle of inclination measured from the xz cross-sectional view (see Fig. 4(b)) over the pellet's lifetime is shown in the inset of Fig. 5(b). In this case, the angle increases for the initial $\approx$ 35 s, represented by the dashed box in the inset of the Fig. 5(b), before it self-balances and reaches a stable position, becoming parallel to the sapphire surface. Owing to the initial tilt of the pellet, the anomalous behavior is exhibited in the vapor layer thickness, characterized by an initial increased measurement within the temporal range during which the pellet maintains its inclination relative to the sapphire surface.

For the majority of the time, excluding the interval characterized by the above-mentioned inclination of the pellet, the predicted values for the vapor layer thickness agree reasonably well with the measured data within the SD. However, a significant deviation between the model predictions and the experimental data can be observed towards the end of the lifetime ($t > 100$ s). This deviation is mainly due to the assumption in the model that the change of the diameter is negligible and only the variation of the pellet's height is considered to be significant during the pellet's lifetime. This assumption is valid for a certain time lapse during the sublimation process, except towards the end, when the pellet starts to shrink in diameter and sublimates rapidly as represented by the circular symbols in Fig. 5(b). As the diameter shrinkage is not taken into account in the model, the bottom surface area of the pellet is over-predicted in the scope of the model. For a given pellet weight, the larger bottom surface area of the pellet requires a lower vapor pressure inside the vapor layer which is associated with the increased vapor layer thickness. Consequently, the model over-predicts the vapor layer thickness when the diameter of the pellet has changed significantly, leading to a theoretically higher vapor layer thickness. Note that for a dry ice pellet the vapor layer thickness increases with time in contrast to Leidenfrost puddles/droplets where the thickness decreases over time and with decreasing size of the droplet as reported in Ref. [19] and [31]. This difference between Leidenfrost solids and liquids is due to the diameter decrease, which is more prominent in liquids than for disc-shaped solids. In the case of Leidenfrost liquids, their shape is controlled by the balance of capillary forces, gravity, and the shear stress in the vapor layer. In contrast, a Leidenfrost solid is rigid and its shape is less sensitive to changes due to external factors. Consequently, the typical bottom surface area for the heat transfer is larger for a disc-shaped Leidenfrost solid than for droplets, implying a higher vapor layer thickness for a given mass of the Leidenfrost object.

The variation of the predicted and measured values of the dimensionless vapor layer thickness (δ^*) normalized by its initial value (δ_0^*) with dimensionless time is shown in Fig. 5(c) for five different sapphire substrate temperatures. Note that the physical time increases from right to left of the x-axis in Fig. 5(c). The predicted values of the dimensionless vapor layer thickness scale with the dimensionless time as $\delta^* \sim (1 - t/\tau)^{-1/3}$ irrespective of the substrate temperature (see Eq. (18) and dashed line in Fig. 5(c)). The dimensionless vapor layer thickness values measured for various substrate temperatures, represented by distinct markers in Fig. 5(c) seem to adhere to this scaling before deviating from the predicted dashed line during the later phase of the pellet's sublimation, attributed to significant shrinkage of the pellet's diameter. In an ideal scenario, all measured data points for the dimensionless vapor layer thickness in Fig. 5(c) should overlap, particularly in the early stages of the pellet's sublimation. However, this is not observed, as the data points diverge from each other and the prediction, resulting in an equivalent dimensional deviation ranging from approximately 3 μm to 6 μm. These deviations may arise from uncontrolled experimental factors, such as the surface roughness of the pellet, the pellet's movement during an OCT acquisition, and the pellet's inclination to the solid substrate, as previously discussed. Despite the non-overlapping nature of the data points, their proximity is evident when considering their SDs, represented by the respective colored bands in Fig. 5(c).

4.3. Vapor layer thickness and pellet lifetime as a function of substrate temperature

This section aims to further clarify findings such as the scaling law for the vapor layer thickness and the lifetime of a pellet as a function of the substrate temperature. Fig. 6(a) shows the initial value of the dimensionless vapor layer thickness (δ_0^*) as a function of the sublimation number (ϵ^*) defined in Eq. (11). The data points correspond to the dimensionless vapor layer thicknesses measured from the first cross-section xz scan (i.e. before 0.17 s elapsed), immediately after the dry ice pellet is placed on the sapphire substrate. These data points are obtained for different initial pellet masses and different substrate temperatures ranging from 30 °C to 70 °C in steps of 10 °C, which in turn means different ϵ^*. The data points are compared with the result of Eq. (18) at a time, $t \approx 0$, according to which the dimensionless vapor layer thickness is proportional to $\epsilon^{*1/4}$. The good agreement between the predicted and measured values seen in Fig. 6 confirms this relation for a disc-shaped dry ice pellet.

In contrast to the relatively uniform vapor layer beneath the dry ice pellet, characterized by a rigid and predetermined shape in the current investigation, the vapor layer profile beneath a Leidenfrost drop assumes a nontrivial configuration based on the radial position. This configuration manifests as a concave depression, termed the "pocket," within the drop interface, bounded by a thinner annular region known as the "neck", as experimentally observed by Burton et al. [20]. Sobac et al. [5] theoretically described this phenomenon by solving for the curvature of the drop interface, accounting for gravity, surface tension, and the hydrostatic pressure variation in the vapor layer, a factor omitted in the earlier work of Pomeau et al. [32]. In analogy to the scaling of the dimensionless vapor layer thickness with the sublimation number (ϵ^*) for the dry ice pellet, the dimensionless thickness of the pocket (h_{center}) and neck (h_{neck}) regions for Leidenfrost droplets are proportional to the evaporation number ($\mathcal{E}$). However, the scaling factors for the Leidenfrost droplets differ from those of the dry ice pellet. Specifically, $h_{center} \sim \mathcal{E}^{1/6}$ and $h_{neck} \sim \mathcal{E}^{1/3}$. Both the sublimation number, defined by Eq. (11), and the evaporation number, as given by Eq. (2) in the work of Sobac et al. [5], are functional properties of the Leidenfrost object and the degree of superheat, denoted as the temperature difference between the substrate and Leidenfrost object ($\Delta T = T_p - T_i$). The distinction between the two numbers lies in their denominators, where the capillary length scale, dependent on the surface tension of the droplet, is present in the formulation of the evaporation number but absent in the sublimation number defined for Leidenfrost solids.

Moreover, a distinct dissimilarity between the Leidenfrost solid and droplet lies in the occurrence of internal convection, particularly evident in the latter, which can significantly influence its Leidenfrost dynamics. The origin of this internal motion may be twofold: it can

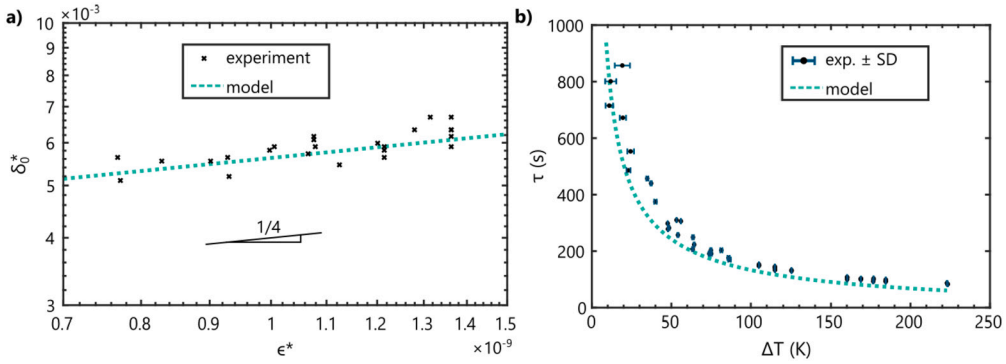

Fig. 6. a) Initial value of the dimensionless vapor layer thickness as a function of the sublimation number. **b)** Lifetime of a disc-shaped dry ice pellet placed on an aluminum substrate as a function of the degree of superheat ΔT.

arise from temperature variations within the Leidenfrost drop or result from the entrainment of liquid by the viscous flow of vapor within the vapor layer, traversing from the droplet's base to its apex. As demonstrated by Bouillant et al. [33], the flow structure inside a Leidenfrost liquid droplet is dependent upon the drop's aspect ratio. A Leidenfrost puddle may exhibit axisymmetric toroidal motion within it, but this symmetry is disrupted as the drop's size diminishes below its capillary length, adopting a quasi-spherical shape and hosting a distinctive roll pattern internally. The swift internal rolling within the quasi-spherical drop is accompanied by the tilting of its base, establishing a ratchet-like mechanism that induces self-propulsion, even on smooth and perfectly horizontal solid substrates. In contrast, in the absence of internal flows, self-propulsion for solid Leidenfrost objects situated on a smooth horizontal surface is achievable only through controlled non-homogeneous mass distribution, leading to a non-uniform vapor layer where vapor flow generates a lateral force propelling the object, as discussed by Dupeux [24].

The model presented in Section 3 is further validated by comparing predicted and measured lifetimes (τ) of the dry ice pellet as a function of the degree of superheat as presented in Fig. 6(b). In this case, the measurements were performed outside the OCT setup, with a dry ice pellet sublimating on an aluminum substrate, to facilitate a wider range of substrate temperatures from -70 °C to 145 °C (Section 2.3). The predicted values shown in Fig. 6(b) are calculated using Eq. (16) which is a typical time scale for the pellet's lifetime for a given substrate temperature, initial mass, and size of the pellet. The temperature-dependent terms appearing in Eq. (16) which increase with increasing substrate temperature are the degree of superheat, vapor thermal conductivity, and dynamic viscosity. Since the pellet's lifetime is proportional to $(\Delta T k_v)^{-3/4}$ and $\mu_v^{1/4}$, the overall effect of an increasing substrate temperature is to decrease the pellet's lifetime for a given initial mass and size of the pellet as seen in Fig. 6(b). In the context of droplets, the so-called Leidenfrost temperature (e.g., 200 °C for millimeter-sized water droplet) at which the levitation typically occurs, characterized by a spike in the lifetime versus substrate temperature curve [19]. However, within the scope of this study, the exploration of whether a critical temperature analogous to the Leidenfrost temperature for droplets exists for dry ice pellets is unexplored. The question persists as to whether only a marginal value of ΔT initiates levitation, driven by the continuous sublimation of the pellet. Addressing this query necessitates a series of experiments conducted with precision, involving controlled substrate temperatures close to the sublimation temperature of dry ice corresponding to a given saturation pressure.

4.4. Time variation of pellet geometry

The lifetime of the dry ice pellet does not provide information on how the pellet sublimates. It is a discrete parameter that only indicates the time elapsed between the pellet being placed on the substrate and its disappearance. To understand the sublimation process, we analyzed the height and diameter evolution of the dry ice pellet over time. The temporal evolution of the height ($h_i = 5$ mm) and diameter ($d_i = 10$ mm) of the dry ice pellet is shown as an example in Fig. 7. The experimental data is obtained from the side-view images of a dry ice pellet captured during sublimation. The solid line and the color band around it represent a quadratic fit to the experimental data of the pellet height and the 95% confidence interval for the fitted parameters, respectively. The measured values of the pellet diameter are represented by square markers. The evolution of the pellet height and diameter are shown for two cases with different substrate temperatures, $T_p \approx$ 323 K and $T_p \approx$ 333 K in Fig. 7(a) and 7(b), respectively. The pellet sublimates faster for higher substrate temperature and its height evolution is similar to the expected evolution as predicted by Eq. (15).

In comparison to the experiments, the rate at which the pellet height decreases is over-predicted by the model as presented in Fig. 7. The difference between predicted and measured values can be ascribed to two main reasons. First, the substrate temperature in the model is assumed to be constant, but in reality, the dry ice pellet will locally cool down the substrate. This causes a reduction in the degree of superheat that leads to a lower sublimation rate induced by a reduced heat transfer rate. That phenomenon can also be deduced from Eq. (15) and (16), depicting that the decrease in the degree of superheating will increase the time scale of the lifetime of the dry ice pellet. Secondly, in the model, the diameter of the pellet is assumed to be constant during the sublimation process. This assumption results in an overestimation of the heat transfer rate from the substrate to the pellet since in reality, the diameter (represented by square markers in Fig. 7) and the surface area decrease over time consequently reducing the heat transfer rate and sublimation rate during the experiment.

5. Conclusion

In present work, the Leidenfrost effect for a disc-shaped dry ice pellet placed on a smooth sapphire substrate was investigated. The spatial profile and the temporal evolution of the vapor layer below the dry ice pellet were revealed for different substrate temperatures by imaging with OCT. The vapor layer thickness was found to be approximately uniform and increased non-linearly as a function of time. This is interestingly in contrast with observations for Leidenfrost liquid drops where the vapor layer profile has distinct pocket and neck regions as measured by Burton et al. [20], and the vapor layer thickness decayed linearly as shown by Biance et al. [19]. In this work, the evolution of the vapor layer thickness and the sublimation of the dry ice pellet were theoretically described in the scope of lubrication approximation, assuming a uniform vapor layer and a constant pellet diameter. The predicted and measured dependence of the initial value of the dimensionless vapor layer thickness on the dimensionless sublimation number are in good agreement. The temporal evolution of the vapor layer thickness, its dimensionless form, and the pellet geometry predicted using the model

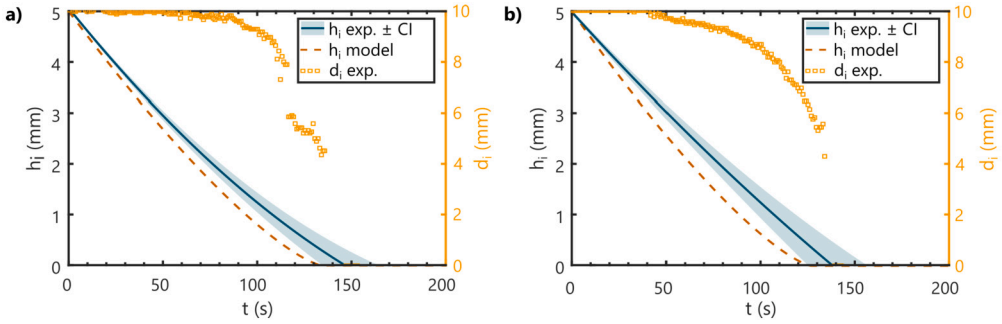

Fig. 7. Time variation of the dry ice pellet height and diameter when it is placed on a hot sapphire substrate at a temperature **a)** $T_p \approx 323$ K, and **b)** $T_p \approx 333$ K. In both plots, solid lines represent experimental height while the bands show the 95% confidence interval (CI), dashed line corresponds to model predictions and square markers indicate the diameter of the pellet.

agree reasonably well with the experimental data for the majority of the sublimation process. Towards the end of the pellet's lifetime, the shrinkage in diameter caused the model to deviate from the experimental data due to the assumption of a constant diameter. As a future perspective, the observations of this work can be used as crucial ingredients for modeling coupled transient behavior of the pellet geometry and the vapor layer thickness to overcome the limitation of the current model in predicting the pellet behavior towards the end of its lifetime. The work presented in this paper can potentially impact several industrial applications as the vapor layer between dry ice and hot substrates is a crucial parameter to control the heat transfer rate.

CRediT authorship contribution statement

A.S. Purandare: Conceptualization, Data curation, Formal analysis, Investigation, Methodology, Validation, Visualization, Writing – original draft. **C. Cuartas-Vélez:** Data curation, Formal analysis, Investigation, Methodology, Software, Validation, Visualization, Writing – original draft. **N. Smeman:** Methodology. **M. Schremb:** Formal analysis, Investigation. **N. Bosschaart:** Funding acquisition, Project administration, Supervision, Writing – review & editing. **S. Vanapalli:** Conceptualization, Funding acquisition, Project administration, Supervision, Writing – review & editing.

Declaration of competing interest

The authors declare that they have no known competing financial interests or personal relationships that could have appeared to influence the work reported in this paper.

Data availability

Data will be made available on request.

Acknowledgements

This work is supported by the tenure-track funding of the Faculty of Science and Technology, the University of Twente to S. Vanapalli. C. Cuartas-Vélez received funding from the Netherlands Organ-on-Chip Initiative (NOCI) (024.003.001).

Appendix A. Supplementary material

Supplementary material related to this article can be found online at https://doi.org/10.1016/j.ijheatmasstransfer.2024.125300.

References

[1] D. Quéré, Leidenfrost dynamics, Annu. Rev. Fluid Mech. 45 (2013) 197–215, https://doi.org/10.1146/annurev-fluid-011212-140709.
[2] L.H. Wachters, H. Bonne, H.J. van Nouhuis, The heat transfer from a hot horizontal plate to sessile water drops in the spherodial state, Chem. Eng. Sci. 21 (1966) 923–936, https://doi.org/10.1016/0009-2509(66)85086-8.
[3] Y.S. Song, D. Adler, F. Xu, E. Kayaalp, A. Nureddin, R.M. Anchan, R.L. Maas, U. Demirci, Vitrification and levitation of a liquid droplet on liquid nitrogen, Proc. Natl. Acad. Sci. USA 107 (2010) 4596–4600, https://doi.org/10.1073/pnas.0914059107.
[4] M. Shirota, M.A. Van Limbeek, C. Sun, A. Prosperetti, D. Lohse, Dynamic leidenfrost effect: relevant time and length scales, Phys. Rev. Lett. 116 (2016) 064501, https://doi.org/10.1103/PhysRevLett.116.064501.
[5] B. Sobac, A. Rednikov, S. Dorbolo, P. Colinet, Leidenfrost effect: accurate drop shape modeling and refined scaling laws, Phys. Rev. E 90 (2014) 053011, https://doi.org/10.1103/PhysRevE.90.053011.
[6] P. Chantelot, D. Lohse, Leidenfrost effect as a directed percolation phase transition, Phys. Rev. Lett. 127 (2021) 124502, https://doi.org/10.1103/PhysRevLett.127.124502.
[7] B. Sobac, A. Rednikov, S. Dorbolo, P. Colinet, Self-propelled leidenfrost drops on a thermal gradient: a theoretical study, Phys. Fluids 29 (2017) 082101, https://doi.org/10.1063/1.4990840.
[8] M. van Limbeek, T. Nes, S. Vanapalli, Impact dynamics and heat transfer characteristics of liquid nitrogen drops on a sapphire prism, Int. J. Heat Mass Transf. 148 (2020) 118999, https://doi.org/10.1016/j.ijheatmasstransfer.2019.118999.
[9] G. Graeber, K. Regulagadda, P. Hodel, C. Küttel, D. Landolf, T.M. Schutzius, D. Poulikakos, Leidenfrost droplet trampolining, Nat. Commun. 12 (2021) 1727, https://doi.org/10.1038/s41467-021-21981-z.
[10] R. Sherman, Chapter 16 - carbon dioxide snow cleaning, in: R. Kohli, K. Mittal (Eds.), Developments in Surface Contamination and Cleaning, second edition, William Andrew Publishing, 2016, pp. 695–716.
[11] J.W. Ong, T. Minifie, E.S. Lin, H.A. Abid, O.W. Liew, T.W. Ng, Cryopreservation without dry ice-induced acidification during sample transport, Anal. Biochem. 608 (2020) 113906, https://doi.org/10.1016/j.ab.2020.113906.
[12] C. Capicciotti, J. Kurach, T. Turner, R. Mancini, J. Acker, R. Ben, Small molecule ice recrystallization inhibitors enable freezing of human red blood cells with reduced glycerol concentrations, Sci. Rep. 5 (2015) 9692, https://doi.org/10.1038/srep09692.
[13] K.R. Byrnes, P.M. Washington, S.M. Knoblach, E. Hoffman, A.I. Faden, Delayed inflammatory mrna and protein expression after spinal cord injury, J. Neuroinflamm. 8 (2011) 130, https://doi.org/10.1186/1742-2094-8-130.
[14] L. Chen, X. Zhang, A review study of solid-gas sublimation flow for refrigeration: from basic mechanism to applications, Int. J. Refrig. 40 (2014) 61–83, https://doi.org/10.1016/j.ijrefrig.2013.11.015.
[15] B. Kochtubajda, E.P. Lozowski, The sublimation of dry ice pellets used for cloud seeding, J. Clim. Appl. Meteorol. 24 (1985) 597–605, https://doi.org/10.1175/1520-0450(1985)024<0597:TSODIP>2.0.CO;2.
[16] G.G. Wells, R. Ledesma-Aguilar, G. McHale, K. Sefiane, A sublimation heat engine, Nat. Commun. 6 (2015) 6390, https://doi.org/10.1038/ncomms7390.
[17] G. Castanet, W. Chaze, O. Caballina, R. Collignon, F. Lemoine, Transient evolution of the heat transfer and the vapor film thickness at the drop impact in the regime of film boiling, Phys. Fluids 30 (2018) 122109, https://doi.org/10.1063/1.5059388.
[18] G.G. Lee, H. Noh, H.J. Kwak, T.K. Kim, H. Park, K. Fezzaa, M.H. Kim, Measurement of the vapor layer under a dynamic leidenfrost drop, Int. J. Heat Mass Transf. 124 (2018) 1163–1171, https://doi.org/10.1016/j.ijheatmasstransfer.2018.04.050.
[19] A. Biance, C. Clanet, D. Quéré, Leidenfrost drops, Phys. Fluids 15 (2003) 1632–1637, https://doi.org/10.1063/1.1572161.
[20] J.C. Burton, A.L. Sharpe, R.C.A. van der Veen, A. Franco, S.R. Nagel, Geometry of the vapor layer under a leidenfrost drop, Phys. Rev. Lett. 109 (2012) 074301, https://doi.org/10.1103/PhysRevLett.109.074301.
[21] G. Lagubeau, M. Le Merrer, C. Clanet, D. Quéré, Leidenfrost on a ratchet, Nat. Phys. 7 (2011) 395–398, https://doi.org/10.1038/nphys1925.
[22] A.G. Marín, D.A. Cerro, G. Römer, B. Pathiraj, A.H. Veld, D. Lohse, Capillary droplets on leidenfrost micro-ratchets, Phys. Fluids 24 (2012) 122001, https://doi.org/10.1063/1.4768813.

[23] T. Baier, G. Dupeux, S. Herbert, S. Hardt, D. Quéré, Propulsion mechanisms for leidenfrost solids on ratchets, Phys. Rev. E 87 (2013) 021001, https://doi.org/10.1103/PhysRevE.87.021001.
[24] G. Dupeux, T. Baier, V. Bacot, S. Hardt, C. Clanet, D. Quéré, Self-propelling uneven leidenfrost solids, Phys. Fluids 25 (2013) 051704, https://doi.org/10.1063/1.4807007.
[25] M. Shi, X. Ji, S. Feng, Q. Yang, T.J. Lu, F. Xu, Self-propelled hovercraft based on cold leidenfrost phenomenon, Sci. Rep. 6 (2016) 1–7, https://doi.org/10.1038/srep28574.
[26] Carboneige | air liquide, https://mygas.airliquide.it/catalog-equipment-products/carboneige. (Accessed 20 October 2022).
[27] C. Veenstra, W. Petersen, I.M. Vellekoop, W. Steenbergen, N. Bosschaart, Spatially confined quantification of bilirubin concentrations by spectroscopic visible-light optical coherence tomography, Biomed. Opt. Express 9 (2018) 3581–3589, https://doi.org/10.1364/BOE.9.003581.
[28] C. Veenstra, W. Kruitwagen, S. Petersen, W. Steenbergen, N. Bosschaart, Quantification of total haemoglobin concentrations in human whole blood by spectroscopic visible-light optical coherence tomography, Sci. Rep. 9 (2019) 15115, https://doi.org/10.1038/s41598-019-51721-9.
[29] C. Cuartas-Vélez, C. Veenstra, W. Kruitwagen, S. Petersen, N. Bosschaart, Optical density based quantification of total haemoglobin concentrations with spectroscopic optical coherence tomography, Sci. Rep. 11 (2021) 8680, https://doi.org/10.1038/s41598-021-88063-4.
[30] A.B. Vakhtin, D.J. Kane, R. Wood, K.A. Peterson, Common-path interferometer for frequency-domain optical coherence tomography, Appl. Opt. 42 (2003) 6953–6958, https://doi.org/10.1364/AO.42.006953.
[31] S. Chandra, S.D. Aziz, Leidenfrost evaporation of liquid nitrogen droplets, J. Heat Transf. 116 (1994) 999–1006, https://doi.org/10.1115/1.2911477.
[32] Y. Pomeau, M. Le Berre, F. Celestini, T. Frisch, The leidenfrost effect: from quasi-spherical droplets to puddles, C. R. Mecanique 34 (2012) 867–881, https://doi.org/10.1016/j.crme.2012.10.034.
[33] A. Bouillant, T. Mouterde, P. Bourrianne, A. Lagarde, C. Clanet, D. Quéré, Leidenfrost wheels, Nat. Phys. 14 (2018) 1188–1192, https://doi.org/10.1038/s41567-018-0275-9.